# Energy localization and topological protection of a locally resonant topological metamaterial for robust vibration energy harvesting

Lan, Chunbo; Hu, Guobiao; Tang, Lihua; Yang, Yaowen

2021

Lan, C., Hu, G., Tang, L. & Yang, Y. (2021). Energy localization and topological protection of a locally resonant topological metamaterial for robust vibration energy harvesting. Journal of Applied Physics, 129(18), 184502-. https://dx.doi.org/10.1063/5.0047965

https://hdl.handle.net/10356/153591

https://doi.org/10.1063/5.0047965

Journal of Applied Physics ARTICLE scitation.org/journal/jap

# Energy localization and topological protection of a locally resonant topological metamaterial for robust vibration energy harvesting

Cite as: J. Appl. Phys. **129**, 184502 (2021); doi: 10.1063/5.0047965
Submitted: 17 February 2021 · Accepted: 24 April 2021 ·
Published Online: 10 May 2021



Chunbo Lan,[1] Guobiao Hu,[2,a)] Lihua Tang,[3] and Yaowen Yang[2]

## AFFILIATIONS

[1]College of Aerospace Engineering, Nanjing University of Aeronautics and Astronautics, Nanjing 210016, China
[2]School of Civil and Environmental Engineering, Nanyang Technological University, 50 Nanyang Avenue, 639798 Singapore, Singapore
[3]Department of Mechanical Engineering, University of Auckland, Auckland 1010, New Zealand

[a)]**Author to whom correspondence should be addressed:** guobiao.hu@ntu.edu.sg

## ABSTRACT

During the past decade, metamaterial-based vibration energy harvesters (meta-VEHs) have been increasingly developed owing to the extraordinary characteristics of metamaterials, such as locally resonant bandgap, defect state, and wave focusing features. In this paper, the interface state, a feature recently found in topological metamaterials, is exploited for low-frequency vibration energy harvesting. The topological meta-VEH consists of two kinds of locally resonant metamaterials with different topological phases and a piezoelectric transducer being installed at the interface between these two metamaterials. First, the governing equations of the topological meta-VEH are established based on the mass–spring model. Subsequently, the dispersion relation of such a one-dimensional topological meta-VEH is obtained by applying Bloch's theorem. It is revealed that the interface mode can be attained in the low-frequency range through the band folding of the locally resonant metamaterial. Moreover, the finitely long model of this topological meta-VEH is built, and the transmittance response is calculated both analytically and numerically. Subsequently, the potential benefits of topological metamaterial, including wave localization and topological protection, are thoroughly investigated. It is found that the elastic energy in the interface state is localized at the interface position, resulting in a significant improvement in output power. Meanwhile, the topological protection property can significantly improve the robustness of the interface mode, thus achieving outstanding energy harvesting performance. Finally, to further enhance the energy harvesting performance, the stiffness tuning method and the defect enhancement method are proposed. It is found that integrating the defect mode and interface mode not only improves the output voltage but also achieves the capability of a highly robust energy harvesting.



## I. INTRODUCTION

Vibration energy harvesting has become one promising method to provide the necessary power for low-power-consumption devices. To efficiently capture the energy from different kinds of vibrations in ambient environments, a variety of energy harvesting mechanisms have been developed during the last two decades.[1–3] At the very beginning, the linear energy harvester received great attention due to its high-power output. However, the operation bandwidth of linear energy harvesters is generally very narrow, which results in low efficiency, as the excitation frequency is away from the resonant frequency of vibration energy harvesters (VEHs).[4] To overcome this problem, researchers introduced stiffness nonlinearity to attain broadband energy harvesting. Various nonlinear energy harvesters have been proposed, such as the Duffing-type VEHs,[5–7] impact-based VEHs,[8] internal resonance-based VEHs,[9] and nonlinearly coupled dual beam systems.[10,11] An in-depth investigation of these nonlinear energy harvesters reveals that the broadband energy harvesting capability can be achieved by capturing and maintaining the high-energy orbit of nonlinear systems. However, these nonlinear systems are sensitive to external perturbations.[12–14] A small disturbance or a minor change of excitation may make a nonlinear system jump from a high-energy orbit to a low-energy one, leading to a low-power output and narrow working band. Therefore, researchers continue to explore innovative mechanisms for efficient vibration energy harvesting.

Metamaterial, which has attracted extensive interest in recent years, has emerged as a new medium for implementing energy harvesting. Metamaterial refers to the material engineered to possess properties that are not observed in natural materials. From the perspective of energy harvesting, the extraordinary properties of metamaterial that can be utilized include locally resonant bandgap, defect state, and wave focusing features. Gonella *et al.*[15] introduced piezoelectric cantilevers into a honeycomb-shaped metamaterial. They demonstrated that these cantilevers could help attain a locally resonant bandgap and convert the wasted mechanical vibration into useful electricity. Mikoshiba *et al.*[16] developed an energy harvesting system with a periodic structure embedded with multiple local resonators. The local resonator is a magnetic energy harvester that consists of a spring-loaded magnet in a capped tube equipped with copper coils. Experimental results showed that the system could generate an output power of 36 mW across a resistive load of 1 Ω. Shen *et al.*[17] designed a metamaterial beam with an array of spiral beams to attain low-frequency bandgaps for low-frequency energy harvesting. Hu *et al.*[18] proposed a metamaterial beam with internally coupled local resonators. The voltage output of the internally coupled metamaterial is four times more than that of the conventional metamaterial. Besides these locally resonant meta-VEHs, the defect mode of metamaterial/phononic crystals (PC) could also be utilized for energy harvesting by concentrating the elastic/acoustic energy at the defect location of metamaterial/PC. Wu *et al.*[19] developed a defect sonic crystal to harvest the acoustic energy. Their experiments show that the power output of the defect PC at a frequency of 4.21 kHz was 24.4 times that of the conventional PC without the defect state. Meanwhile, Carrara *et al.*[20] utilized metamaterial with an intentionally designed defect for vibration energy harvesting. It was found that the harvested power was at the microwatt level, which is much higher than that of acoustic energy harvesting. Carrara *et al.*[21] developed a mirror-type PC plate to enhance the energy harvesting capability. It was found that the acoustic mirror effect could focus the wave energy to a specific point, and the output power was increased by more than one order of magnitude as compared with the plain plate. Tol *et al.*[22] proposed a gradient-index PC lens-based VEH, which can focus the wave at a focal spot by customizing the refractive index. It was found that the wave focusing effect took place over a wide frequency range, and the energy harvesting efficiency was increased by 13.8 times as compared with a plain plate. Further investigation of the above metamaterial/PC-based vibration energy harvesters (meta-VEHs) revealed that wave localization and focusing are the keys to attain outstanding energy harvesting performance. However, it was also found that the efficiencies of the above mechanisms are quite sensitive to the defect (such as structural damage and fatigue), which may lead to a significant reduction in energy output. In short, improving the robustness of meta-VEHs remains a critical problem to be solved.

Meanwhile, topological metamaterial has become one of the most attractive and interesting research areas during the last 5 years.[23] The topological edges and interface states have attracted extensive attention, since the topologically protected interface modes are immune to lattice defects, which is of great interest for robust wave guiding and focusing.[24–26] In particular, the interface mode of topological metamaterial is a promising candidate to attain robust vibration energy harvesting. Although no research on topological-metamaterial-based vibration energy harvesting has been reported, a pioneering work of using topological PC to harvest acoustic energy can give a glimpse of the potential benefits of topological metamaterials. Recently, Fan *et al.*[27] designed a topological PC with a piezoelectric transducer attached at the interface. Their simulation results indicated that the acoustic pressure at the interface was amplified by 66 times, and an output power of 135 mW was generated at the eigenfrequency of the interface mode (4045 Hz). However, for vibration energy harvesting, the vibration source frequency is relatively low in general. Hence, the topological PC is no longer suitable for low-frequency vibration energy harvesting. Meanwhile, the benefits of the unique features of topological metamaterials for vibration energy harvesting are still an open question to be explored. To this end, this paper is motivated to develop a novel VEH based on the locally resonant topological metamaterial to achieve low-frequency energy harvesting, and to study the potential benefits of the wave localization and topological protection features on improving the efficiency and robustness of energy harvesting. Moreover, two different methods to enhance the performance of topological meta-VEH are proposed. The main contents of this paper are organized as follows. Section II depicts the design strategy of locally resonant topological meta-VEH and establishes its electromechanical governing equations. Section III derives the analytical solutions of the topological meta-VEH and studies its band structure and transmittance features. Section IV explores the benefits of the interface mode and topological protection for vibration energy harvesting. Moreover, performance-enhanced methods are proposed in Sec. V to further improve the wave localization effect and the output voltage. Several conclusions are drawn in Sec. VI.

## II. TOPOLOGICAL META-VEH MODEL

### A. System description

For a one-dimensional (1D) topological metamaterial, there are two topologically distinct 1D metamaterials, and the topological interface state takes place at the junction of these two metamaterials. To design a 1D topological metamaterial, the Su–Schrieffer–Heeger (SSH) model[28] has been widely used. For example, Yin *et al.*[29] proposed an elastic PC based on the SSH model and obtained the topological edge mode numerically and experimentally. Muhammad *et al.*[30] proposed a topological PC beam based on the SSH model and studied its topological interface mode. Meanwhile, the local resonance mechanism is utilized to achieve the topological interface mode at the low-frequency range. For example, Zhao *et al.*[31] proposed a topological metamaterial with local resonators. The topological interface mode takes place in the lowest bandgap, i.e., the band-folding induced bandgap. Therefore, the eigenfrequency of the topological interface mode is lower than the natural frequency of the local resonator. In other words, the topological interface mode can be designed in the subwavelength region for low-frequency applications. Hence, a locally resonant topological metamaterial is employed for vibration energy harvesting in this paper.

Figure 1 depicts the schematic of the proposed topological meta-VEH. It consists of two topologically distinct metamaterials,

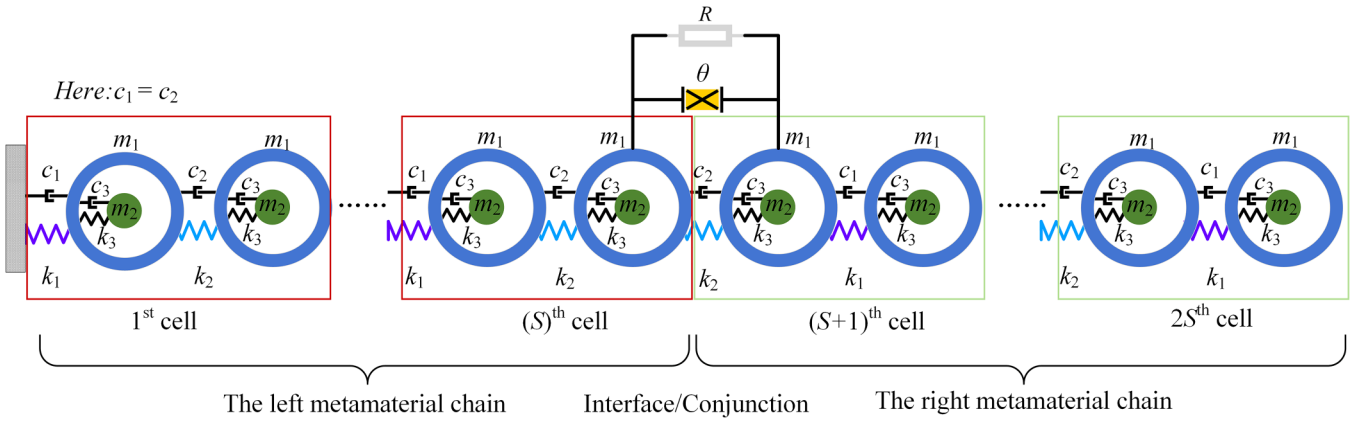


**FIG. 1.** Schematic of a locally resonant topological meta-VEH.

i.e., the left metamaterial chain (marked by the red boxes) and the right metamaterial chain (marked by the green boxes). The *Zak* phase[32] can be used to identify the topology of these two submetamaterial chains. The dashed boxes mark the unit cells for these two submetamaterials. It is noted that the structures of these two kinds of unit cells are quite similar. The unit cells in both submetamaterial chains consist of a diatomic chain with $k_1 \neq k_2$. The main difference is that $k_1$ and $k_2$ are swapped in these unit cells. Such a difference[31,33] is the key for changing the topological invariant of the submetamaterial chains and ensuring that the topological interface mode takes place at the junction of these two submetamaterial chains. Section III will discuss the details of the band structure and topology features. To harvest the vibration energy, a piezoelectric transducer is attached at the interface since the elastic wave is localized there, and a large deformation can be guaranteed. The resistive load $R$ is connected to the piezoelectric transducer to evaluate the harvested power.

### B. Governing equations

The governing equations of the proposed topological meta-VEH are derived based on Newton's second law and Kirchhoff's law. The left, right, and the conjunction boundary conditions of the topological metamaterial are different, leading to different constraint equations. Hence, the whole system is divided into six parts, and their governing equations are given separately. For an arbitrary unit cell in the middle of the left metamaterial chain, the governing equations are

$$\begin{cases} \left[\begin{array}{l} m_1\ddot{u}_1^{2i+1} + c_1(\dot{u}_1^{2i+1} - \dot{u}_1^{2i}) - c_2(\dot{u}_1^{2i+2} - \dot{u}_1^{2i+1}) + c_3(\dot{u}_1^{2i+1} - \dot{u}_2^{2i+1}) \\ \quad + k_1(u_1^{2i+1} - u_1^{2i}) - k_2(u_1^{2i+2} - u_1^{2i+1}) + k_3(u_1^{2i+1} - u_2^{2i+1}) \end{array}\right] = 0, \\ m_2\ddot{u}_2^{2i+1} + c_3(\dot{u}_2^{2i+1} - \dot{u}_1^{2i+1}) + k_3(u_2^{2i+1} - u_1^{2i+1}) = 0, \\ \left[\begin{array}{l} m_1\ddot{u}_1^{2i+2} + c_2(\dot{u}_1^{2i+2} - \dot{u}_1^{2i+1}) - c_1(\dot{u}_1^{2i+3} - \dot{u}_1^{2i+2}) + c_3(\dot{u}_1^{2i+2} - \dot{u}_2^{2i+2}) \\ \quad + k_2(u_1^{2i+2} - u_1^{2i+1}) - k_1(u_1^{2i+3} - u_1^{2i+2}) + k_3(u_1^{2i+2} - u_2^{2i+2}) \end{array}\right] = 0, \\ m_2\ddot{u}_2^{2i+2} + c_3(\dot{u}_2^{2i+2} - \dot{u}_1^{2i+2}) + k_3(u_2^{2i+2} - u_1^{2i+2}) = 0, \end{cases} \tag{1}$$

where $i = 1 \sim S-2$, $m_1$ and $m_2$ denote the outer and inner masses, respectively; $c_1$, $c_2$, and $c_3$ are the corresponding damping coefficients; $k_1$, $k_2$, and $k_3$ are the spring constants. $u_1^n$ and $u_2^n$ denote the displacements of the outer and inner masses, respectively, where the superscripts $n = 2i+1$, $2i+2$, denote the two neighboring modules in the $(i+1)$th unit cell.

For the first unit cell of the left metamaterial chain (i.e., $i = 0$), the governing equations are

$$\begin{cases} m_1\ddot{u}_1^1 + c_1\dot{u}_1^1 - c_2(\dot{u}_1^2 - \dot{u}_1^1) + c_3(\dot{u}_1^1 - \dot{u}_2^1) + k_1(u_1^1 - u_1^0) - k_2(u_1^2 - u_1^1) + k_3(u_1^1 - u_2^1) = 0, \\ m_2\ddot{u}_2^1 + c_3(\dot{u}_2^1 - \dot{u}_1^1) + k_3(u_2^1 - u_1^1) = 0, \\ m_1\ddot{u}_1^2 + c_2(\dot{u}_1^2 - \dot{u}_1^1) - c_1(\dot{u}_1^3 - \dot{u}_1^2) + c_3(\dot{u}_1^2 - \dot{u}_2^2) + k_2(u_1^2 - u_1^1) - k_1(u_1^3 - u_1^2) + k_3(u_1^2 - u_2^2) = 0, \\ m_2\ddot{u}_2^2 + c_3(\dot{u}_2^2 - \dot{u}_1^2) + k_3(u_2^2 - u_1^2) = 0, \end{cases} \tag{2}$$

where $u_1^0$ denotes the base displacement applied to the left-hand side of the whole metamaterial. For the ($S$)th unit cell (i.e., $i = S-1$), the governing equations are

$$\begin{cases} \left[\begin{array}{l} m_1\ddot{u}_1^{2S-1} + c_1(\dot{u}_1^{2S-1} - \dot{u}_1^{2S-2}) - c_2(\dot{u}_1^{2S} - \dot{u}_1^{2S-1}) + c_3(\dot{u}_1^{2S-1} - \dot{u}_2^{2S-1}) \\ \quad + k_1(u_1^{2S-1} - u_1^{2S-2}) - k_2(u_1^{2S} - u_1^{2S-1}) + k_3(u_1^{2S-1} - u_2^{2S-1}) \end{array}\right] = 0, \\ m_2\ddot{u}_2^{2S-1} + c_3(\dot{u}_2^{2S-2+1} - \dot{u}_1^{2S-2+1}) + k_3(u_2^{2S-2+1} - u_1^{2S-2+1}) = 0, \\ \left[\begin{array}{l} m_1\ddot{u}_1^{2S} + c_2(\dot{u}_1^{2S} - \dot{u}_1^{2S-1}) - c_2(\dot{u}_1^{2S+1} - \dot{u}_1^{2S}) + c_3(\dot{u}_1^{2S} - \dot{u}_2^{2S}) \\ \quad + k_2(u_1^{2S} - u_1^{2S-1}) - k_2(u_1^{2S+1} - u_1^{2S}) + k_3(u_1^{2S} - u_2^{2S}) - \theta v \end{array}\right] = 0, \\ m_2\ddot{u}_2^{2S} + c_3(\dot{u}_2^{2S} - \dot{u}_1^{2S}) + k_3(u_2^{2S} - u_1^{2S}) = 0, \end{cases} \tag{3}$$

where $\theta$ is the electromechanical coupling coefficient and $v$ is the output voltage. For an arbitrary unit cell in the middle of the right metamaterial chain, the governing equations are

$$\begin{cases} \left[\begin{array}{l} m_1\ddot{u}_1^{2i+1} + c_2(\dot{u}_1^{2i+1} - \dot{u}_1^{2i}) - c_1(\dot{u}_1^{2i+2} - \dot{u}_1^{2i+1}) + c_3(\dot{u}_1^{2i+1} - \dot{u}_2^{2i+1}) \\ \quad + k_2(u_1^{2i+1} - u_1^{2i}) - k_1(u_1^{2i+2} - u_1^{2i+1}) + k_3(u_1^{2i+1} - u_2^{2i+1}) \end{array}\right] = 0, \\ m_2\ddot{u}_2^{2i+1} + c_3(\dot{u}_2^{2i+1} - \dot{u}_1^{2i+1}) + k_3(u_2^{2i+1} - u_1^{2i+1}) = 0, \\ \left[\begin{array}{l} m_1\ddot{u}_1^{2i+2} + c_1(\dot{u}_1^{2i+2} - \dot{u}_1^{2i+1}) - c_2(\dot{u}_1^{2i+3} - \dot{u}_1^{2i+2}) + c_3(\dot{u}_1^{2i+2} - \dot{u}_2^{2i+2}) \\ \quad + k_1(u_1^{2i+2} - u_1^{2i+1}) - k_2(u_1^{2i+3} - u_1^{2i+2}) + k_3(u_1^{2i+2} - u_2^{2i+2}) \end{array}\right] = 0, \\ m_2\ddot{u}_2^{2i+2} + c_3(\dot{u}_2^{2i+2} - \dot{u}_1^{2i+2}) + k_3(u_2^{2i+2} - u_1^{2i+2}) = 0, \end{cases} \tag{4}$$

where $i = S+1 \sim 2S-2$. For the first unit cell of the right metamaterial chain (i.e., $i = S$), the governing equations are

$$\begin{cases} \left[\begin{array}{l} m_1\ddot{u}_1^{2S+1} + c_2(\dot{u}_1^{2S+1} - \dot{u}_1^{2S}) - c_1(\dot{u}_1^{2S+2} - \dot{u}_1^{2S+1}) + c_3(\dot{u}_1^{2S+1} - \dot{u}_2^{2S+1}) \\ \quad + k_2(u_1^{2S+1} - u_1^{2S}) - k_1(u_1^{2S+2} - u_1^{2S+1}) + k_3(u_1^{2S+1} - u_2^{2S+1}) + \theta v \end{array}\right] = 0, \\ m_2\ddot{u}_2^{2S+1} + c_3(\dot{u}_2^{2S+1} - \dot{u}_1^{2S+1}) + k_3(u_2^{2S+1} - u_1^{2S+1}) = 0, \\ \left[\begin{array}{l} m_1\ddot{u}_1^{2S+2} + c_1(\dot{u}_1^{2S+2} - \dot{u}_1^{2S+1}) - c_2(\dot{u}_1^{2S+3} - \dot{u}_1^{2S+2}) + c_3(\dot{u}_1^{2S+2} - \dot{u}_2^{2S+2}) \\ \quad + k_1(u_1^{2S+2} - u_1^{2S+1}) - k_2(u_1^{2S+3} - u_1^{2S+2}) + k_3(u_1^{2S+2} - u_2^{2S+2}) \end{array}\right] = 0, \\ m_2\ddot{u}_2^{2S+2} + c_3(\dot{u}_2^{2S+2} - \dot{u}_1^{2S+2}) + k_3(u_2^{2S+2} - u_1^{2S+2}) = 0. \end{cases} \tag{5}$$

For the last unit cell of the right metamaterial chain (i.e., $i = 2S-1$), the governing equations are

$$\begin{cases} \left[\begin{array}{l} m_1\ddot{u}_1^{4S-1} + c_2(\dot{u}_1^{4S-1} - \dot{u}_1^{4S-2}) - c_1(\dot{u}_1^{4S} - \dot{u}_1^{4S-1}) + c_3(\dot{u}_1^{4S-1} - \dot{u}_2^{4S-1}) \\ \quad + k_2(u_1^{4S-1} - u_1^{4S-2}) - k_1(u_1^{4S} - u_1^{4S-1}) + k_3(u_1^{4S-1} - u_2^{4S-1}) \end{array}\right] = 0, \\ m_2\ddot{u}_2^{4S-1} + c_3(\dot{u}_2^{4S-1} - \dot{u}_1^{4S-1}) + k_3(u_2^{4S-1} - u_1^{4S-1}) = 0, \\ m_1\ddot{u}_1^{4S} + c_1(\dot{u}_1^{4S} - \dot{u}_1^{4S-1}) + c_3(\dot{u}_1^{4S} - \dot{u}_2^{4S}) + k_1(u_1^{4S} - u_1^{4S-1}) + k_3(u_1^{4S} - u_2^{4S}) = 0, \\ m_2\ddot{u}_2^{4S} + c_3(\dot{u}_2^{4S} - \dot{u}_1^{4S}) + k_3(u_2^{4S} - u_1^{4S}) = 0. \end{cases} \tag{6}$$

Assuming the piezoelectric transducer is shunted to a resistive load $R$, the governing equation of the electrical domain is

$$\frac{v}{R} + C_p\dot{v} + \theta(\dot{u}_1^{2S+1} - \dot{u}_1^{2S}) = 0, \tag{7}$$

where $C_p$ is the capacitance of the piezoelectric transducer.

## III. BAND STRUCTURE AND TRANSMITTANCE ANALYSES

In this section, the band structure features of the proposed topological meta-VEH are studied. The band inversion and topology properties are discussed to provide insights into the potential advantages of topological meta-VEH. Subsequently, the transmittance and output voltage of the proposed meta-VEH are derived analytically, laying the foundation for Secs. IV and V. Figure 2 depicts the unit cell of the metamaterial. The methods of calculating the band structure and transmittance are provided in the Appendix. The parameters of the metamaterial system studied in this paper are listed in Table I.

### A. Band structure

Figure 3 plots the dispersion relations of the locally resonant metamaterial for different $k_l$ and $k_r$. It is found that when $k_l = k_r$

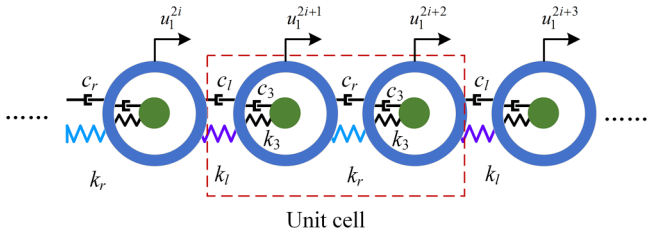


**FIG. 2.** Unit cell of the metamaterial.

(conventional metamaterial chain), there is only one locally resonant bandgap (LRBG), as shown in Fig. 3(b). When $k_l = 8000$ N/m and $k_r = 4000$ N/m ($k_l > k_r$, the left metamaterial chain), except for the LRBG, two more Bragg Scattering bandgaps (BSBGs) [Fig. 3(a)] are opened from the band-folding points [P1 and P2 in Fig. 3(b)]. Notably, the first BSBG is lower than the LRBG. Since the topological interface mode occurs inside these band-folding induced bandgaps, the interface mode can be achieved at the low-frequency range by a locally resonant topological metamaterial. Thus, it can be used for low-frequency energy harvesting. When the values of $k_1$ and $k_2$ are swapped ($k_l < k_r$, the right metamaterial chain), the dispersion relation shown in Fig. 3(c) is exactly the same as that in Fig. 3(a). In other words, the absolute eigenfrequencies of these two configurations are the same, which validates the analytical predictions of Eq. (A5).

Subsequently, Table II shows the eigenvectors of the left and right metamaterial chains at the edges of the first bandgap. It is found that at state 1 ($qL = \pi$, $\omega/\omega_n = 0.5996$, related to S1 and S3 of Fig. 3), the eigenvector of the outer masses of left metamaterial chain ($k_l > k_r$) is (1,1), while that of right metamaterial chain ($k_l < k_r$) is (−1,1). At state 2 ($qL = \pi$, $\omega/\omega_n = 0.7808$, related to S2 and S4 of Fig. 3), the eigenvector of left metamaterial chain becomes (−1,1), while that of right metamaterial chain turns to be (1,1). Thus, the band inversion induced by the exchange of $k_1$ and $k_2$ occurs in the first bandgap. To illustrate the benefit of band inversion for wave localization and energy harvesting, the mode shapes of these two configurations and the topological metamaterial are plotted in Fig. 4. For the left metamaterial chain, the lower band edge S1 (1, 1) corresponds to an even mode, and the directions of mass motions in a unit cell are the same. For the right metamaterial chain, at the band edge S3 (−1, 1), although the frequency does not change, the directions of mass motions in a unit cell turn to be opposite to each other. Assume that these two configurations of metamaterials are integrated to form a new metamaterial (as shown in Fig. 4), the wave energy can be localized at the conjunction due to the band inversion, resulting in a large deformation. Thus, if a piezoelectric patch is mounted at the interface, high efficiency of energy harvesting can be achieved.

The second possible advantage of the proposed meta-VEH originates from the topological protection property. It is well known that vibration energy localization can be attained in a defected metamaterial as well. However, the defect mode is strongly dependent on the defect property. In a defected metamaterial, the fatigue and damage of structures may result in the loss of the defect mode and wave energy localization. Unlike the defected metamaterial, the interface mode mainly depends on the structural topology property. The wave localization property and interface mode of a topological metamaterial always exist, and they are immune to structural fatigue and damage if the topology properties of the metamaterial remain constant. For a 1D topological metamaterial, its topology property can be identified by the topological invariant, i.e., the *Zak* phase, which can be calculated using the following formula:

$$\theta_{zak} = i\int_{-\pi/L}^{\pi/L} dq\langle\Psi|\partial_q|\Psi\rangle = -\frac{\phi(\pi/L) - \phi(-\pi/L)}{2} = \begin{cases} \pi, & k_l < k_r, \\ 0, & k_l > k_r, \end{cases} \tag{8}$$

where $|\Psi\rangle$ is the eigenvector normalized by the kinetic energy. The details about *Zak*-phase calculations can be found in Ref. 31. From Eq. (8), it is learned that the *Zak* phases for all the bands of the left metamaterial chain are the same, equaling 0, while all the bands of the right metamaterial chain have the same *Zak* phase π. The *Zak* phase value indicates that the metamaterial used for energy harvesting (shown in Fig. 1) is a topological one, which is immune to structural defects. More specifically, since the interface mode depends on the topology features and a local defect can hardly change the topology feature of the whole metamaterial, the local defect may change the frequency of the topological interface state but cannot eliminate the topological interface mode. Moreover, the wave localization position of interface mode always locates at the interface regardless of the local defect. Section IV will provide an in-depth study on the advantages of topological protection for vibration energy harvesting.

**TABLE I.** Parameters of the topological meta-VEH.

| Parameters | Value | Parameters | Value |
|---|---|---|---|
| Outer mass $m_1$ (kg) | 0.004 | Capacitance $C_p$ (nF) | 187 |
| Inner mass $m_2$ (kg) | 0.001 | Electromechanical coupling (mN/V) | 0.6 |
| $k_1$ (N/m) | 8000 | $c_1$ (N s/m) | 0.001 |
| $k_2$ (N/m) | 4000 | $c_2$ (N s/m) | 0.001 |
| $k_3$ (N/m) | 4000 | $c_3$ (N s/m) | 0.05 |
| Resistance (kΩ) | 10 000 | | |

## B. Transmittance

Figure 5 compares the transmittance and dispersion relations of the topological meta-VEH. It is clearly shown that the transmittance agrees quite well with the predicted band structure. There are two BSBGs and one LRBG. As predicted, the interface mode marked with a blue star is observed inside the first BSBG. Meanwhile, it is also revealed that such an interface mode can be designed in the low-frequency range by introducing the local resonators, making it suitable for low-frequency vibration energy harvesting.

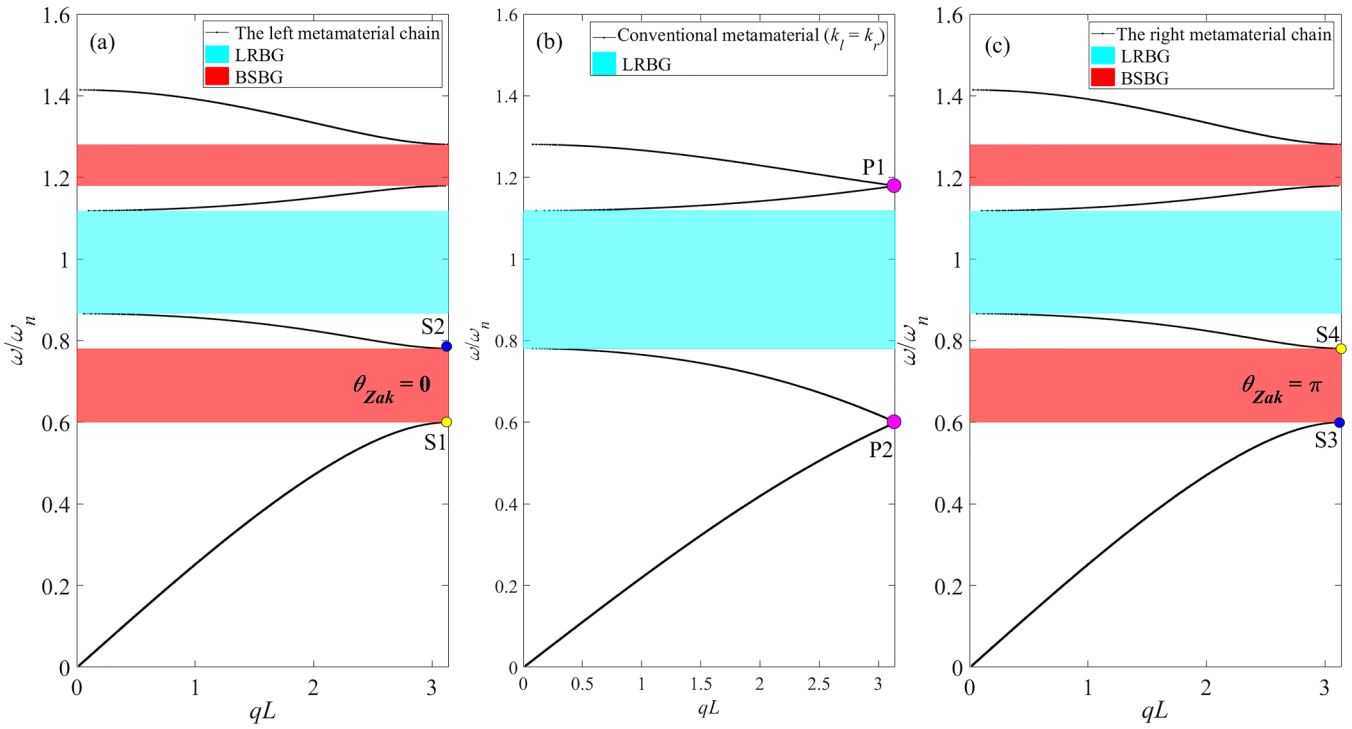


**FIG. 3.** Dispersion relations of the unit cell for different configurations [$k_1 = 8000$ N/m, $k_2 = 4000$ N/m, $\omega_n = (k_3/m_2)^{1/2}$]: (a) left metamaterial chain, $k_l = k_1$, $k_r = k_2$, (b) conventional metamaterial chain, $k_l = k_r = k_1$, (c) right metamaterial chain, $k_l = k_2$, $k_r = k_1$.

## IV. ENERGY HARVESTING PERFORMANCE

In this section, the performance of a topological meta-VEH for energy harvesting is studied. There are mainly two aspects: one is the benefit of wave localization for energy harvesting, while the other is the benefit of topological protection. The parameters used in this section are the same as those in Table I.

### A. Benefit of wave localization of the interface mode

To illustrate the advantages of wave localization in the interface mode for vibration energy harvesting, the displacement responses of the topological meta-VEH are calculated, as shown in Fig. 6. For the proposed topological meta-VEH, there are mainly two configurations. The first one, named as configuration A, refers to the one that the left metamaterial has $k_l > k_r$ while the right metamaterial has $k_r < k_l$. The second one, named configuration B, refers to the one which exchanges the left and right metamaterials. From Fig. 6, it is learned that the displacement distributions of configuration A are just like an isosceles triangle, and the maximum response appears at the interface. Thus, the vibration is successfully localized at the interface. For configuration B, a similar displacement distribution is obtained, and the wave energy is also localized at the interface. The main difference between these two configurations is the location of the maximum displacement. The maximum response of configuration A occurs at the $2S$th module, while that of configuration B appears at the $(2S-1)$th and $(2S+1)$th

**TABLE II.** Eigenvector of different configurations.

| Parameters | Eigenvector | |
|---|---|---|
| | Left metamaterial chain ($k_l > k_r$) | Right metamaterial chain ($k_1 < k_2$) |
| | $(u_1^{2i+1}, u_1^{2i+2}, u_2^{2i+1}, u_2^{2i+2}) = \left(\pm e^{i\phi(q)}, 1, \pm \frac{k_3}{k_3 - m\omega^2} e^{i\phi(q)}, \frac{k_3}{k_3 - m\omega^2}\right)$ (Ref. 31) | |
| $qL = \pi$, $\omega/\omega_n = 0.5996$ | S1, $\left(1, 1, \frac{k_3}{k_3 - m\omega^2}, \frac{k_3}{k_3 - m\omega^2}\right)$ | S3, $\left(-1, 1, -\frac{k_3}{k_3 - m\omega^2}, \frac{k_3}{k_3 - m\omega^2}\right)$ |
| $qL = \pi$, $\omega/\omega_n = 0.7808$ | S2, $\left(-1, 1, -\frac{k_3}{k_3 - m\omega^2}, \frac{k_3}{k_3 - m\omega^2}\right)$ | S4, $\left(1, 1, \frac{k_3}{k_3 - m\omega^2}, \frac{k_3}{k_3 - m\omega^2}\right)$ |

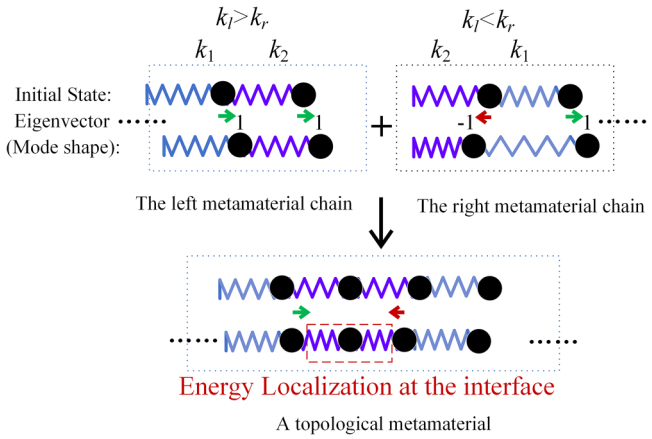


**FIG. 4.** Conceptual illustration of energy localization at the interface of a topological metamaterial.

modules. Therefore, the piezoelectric transducers should be mounted at different places for these two configurations. For configuration A, the piezoelectric transducer is recommended to be placed at the 2*S*th module, while for configuration B, it is recommended to be placed between the $(2S-1)$th and $(2S)$th modules, or the $(2S+1)$th and $(2S+2)$th modules since the voltage is closely related to the relative displacement between the neighboring modules. From the displacement distribution, it is clearly found that the maximum relative displacement of configuration A is about 8.28, while that of configuration B is only 1.05. Thus, we can conclude that although there is only one maximum peak in configuration A, the capability of energy localization of configuration A is superior to configuration B.

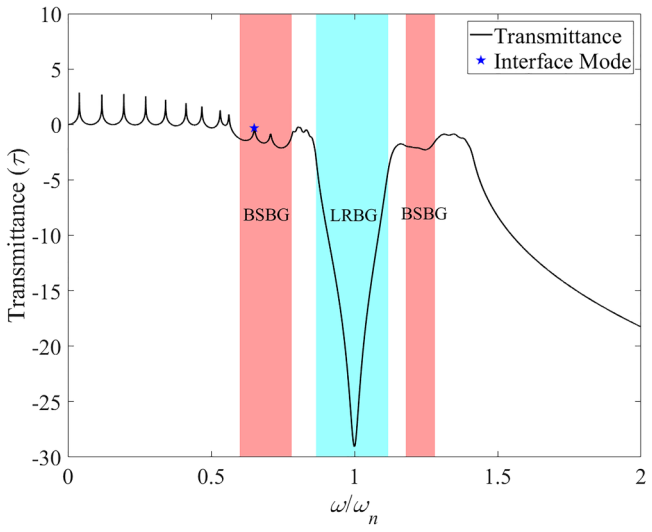


**FIG. 5.** Transmittance and interface mode of a topological metamaterial.

Subsequently, the relations between the resistance load and power of these two configurations are obtained to evaluate the power performance. Since the varying resistance load can affect the resonant frequency of the topological interface mode, the excitation frequency related to the peak power is different as well. To obtain the peak power at different resistance loads, we first obtain the frequency–voltage response for different resistance loads. For each resistance load, the resonance peak related to the interface mode is recognized and used to calculate the power peak. Figures 7(a) and 7(b) compare the generated power of these two configurations. The peak power of configuration A is about 2.169 mW, while that of configuration B is only 0.019 33mW. The optimal resistance loads for configurations A and B are different. The optimal resistance of configuration A is 4.2 kΩ while that of configuration B is 3.8 kΩ. To evaluate the energy harvesting efficiency, the outputted power should be normalized with respect to the inputted power. Figures 7(c) and 7(d) depict the normalized power of these two configurations, it is found that the maximum energy harvesting efficiency of configuration A is 0.0208% while that of configuration B is 0.000 68%. Notably, the energy harvesting efficiency is quite low since the electromechanical coupling is very weak in this example, resulting in a very weak electromechanical conversion efficiency. To improve the energy harvesting efficiency, one can increase the electromechanical conversion efficiency by increasing the size and improving the quality of the piezoelectric transducer. Overall speaking, the energy harvesting performance of configuration A is much better than that of configuration B, even though both configurations can localize energy at the interface.

### B. Benefit of topological protection

In this section, a conventional defected meta-VEH and the proposed topological meta-VEH are compared to illustrate the benefit of topological protection for energy harvesting performance. It is assumed that the defects locate at the center of the three meta-VEHs. The $(2S)$th module's stiffness ($k_{2S}$) of configuration A is regarded as the defect stiffness since the structural fatigue or damage is most likely to appear at the location of energy localization. To distinguish a defect mode curve from a series of ordinary mode curves, the modal shapes of these curves are examined. For a defect mode, the energy should be localized at the defect place. Therefore, there will be a peak at the defected cell in the displacement distribution response. We have examined the distribution responses at several specific points associated with those curves to figure out their characteristics. The defected topological metamaterial and the conventional defected meta-VEHs are illustrated on the top of Fig. 8. Then, the eigenfrequency of topological interface mode for varying $k_{2S}$ is depicted in Fig. 8(a), while that of the defect mode for varying $k_{2S}$ or $k_{2S+1}$ is shown in Figs. 8(b) and 8(c), respectively. It is found in Fig. 8(a) that, for the topological meta-VEH, when the defected stiffness $k_{2S}$ increases from zero to $3k_3$, the resonance frequency of interface mode will increase but is still inside the first BSBG. However, for the conventional meta-VEH with a defected stiffness ($k_{2S}$ or $k_{2S+1}$), the defect mode may disappear sometimes. For the first configuration of conventional meta-VEHs [Fig. 8(b)], it is found that when $k_{2S} < k_3$, there is no defect mode. For the second configuration of conventional

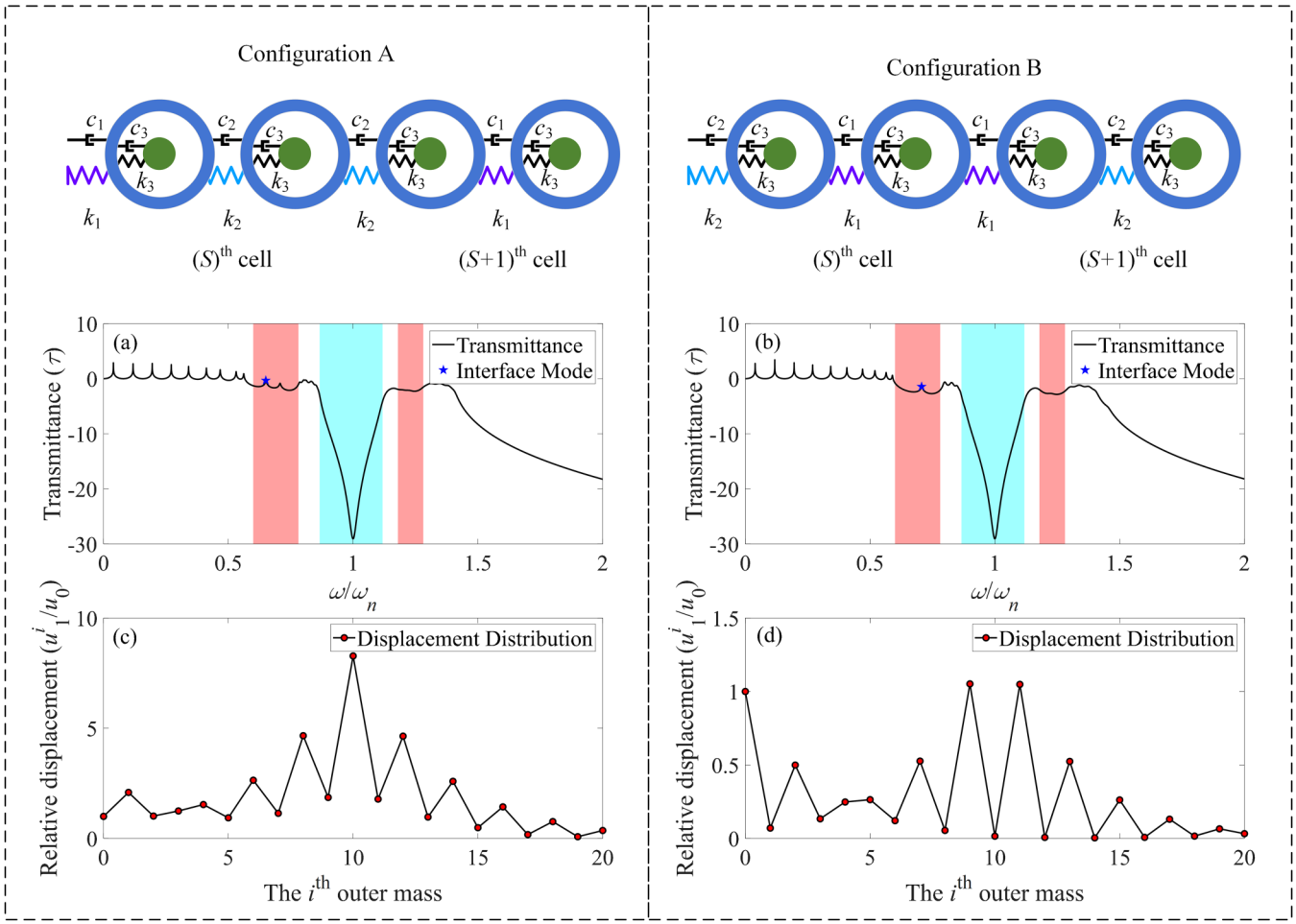


**FIG. 6.** Transmittance, interface mode, and displacement distributions of two different configurations of topological metamaterials (20 modules and 10 unit cells, $S = 5$, $k_1 > k_2$): (a) and (b) are the transmittances and (c) and (d) are the displacement distributions.

meta-VEHs [Fig. 8(c)], the defect mode will disappear when $k_{2S+1} > 2k_3$. Thus, it is clearly revealed that the topological interface is more robust than the defect mode, which indicates that the topological meta-VEH has the capability of achieving the robustness for vibration energy harvesting.

## V. PERFORMANCE ENHANCEMENT STRATEGIES

Section IV has clearly shown the advantages of topological metamaterial for robust vibration energy harvesting. In this section, we are motivated to seek strategies to further enhance the performance of the proposed topological meta-VEH.

### A. Stiffness tuning approach

The first strategy is to tune the spring constants of the topological metamaterial, named stiffness tuning approach hereinafter. The details of this approach are depicted as follows. The stiffness constants in the two configurations of topological meta-VEH, as shown in Fig. 9, are tuned to $k_t$, which is varied from 1600 to 5200 N/m. The excitation amplitude $u_0$ and other parameters are the same as those in Table I. The effects of $k_t$ on the three aspects of interest related to energy harvesting, i.e., the eigenfrequency, the displacement distribution, and the output voltage of the topological meta-VEHs, are investigated.

Figures 9(c) and 9(d) reveal the effects of $k_t$ on the eigenfrequencies of the interface modes and the voltage outputs of the two topological meta-VEHs. It is found that for both configurations of topological meta-VEHs, their eigenfrequencies and voltage outputs increase with $k_t$. In other words, a small stiffness $k_t$ helps reduce the resonant frequency, which is beneficial for low-frequency energy harvesting. However, the output voltage is unfavorably decreased at the same time. Therefore, it is suggested to reduce the natural frequency of local resonators rather than the stiffness of the main structure. To ascertain the reason for the decreasing output

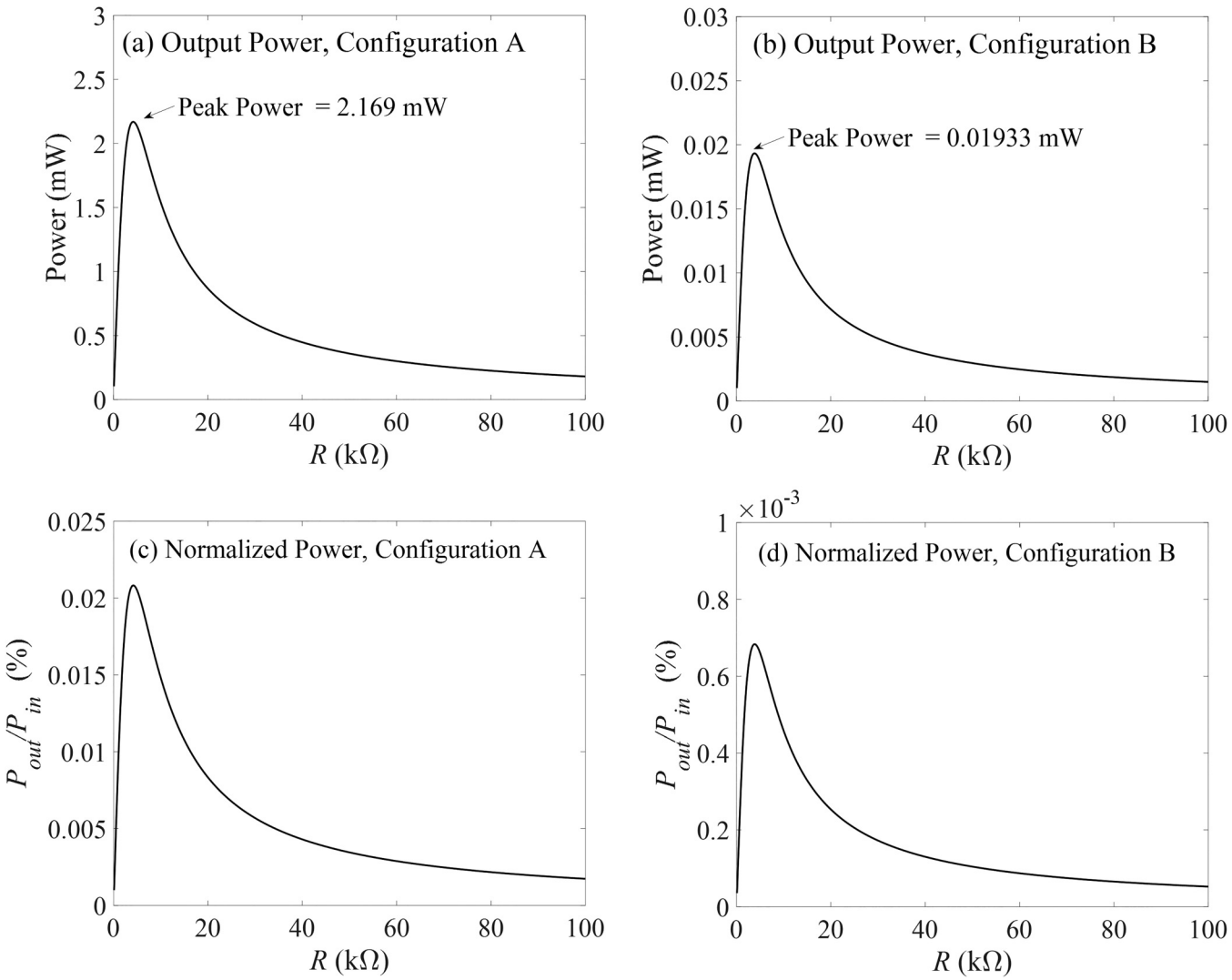


**FIG. 7.** Power performance of two different configurations of topological meta-VEH ($u_0 = 0.001$): $P_{out}$ and $P_{in}$ are the outputted power and the inputted power, respectively.

voltage, the displacement distribution at the topological interface modes of the two configurations is plotted in Figs. 9(e) and 9(f). It is found that with the increase in stiffness $k_t$, the displacement amplitude at the interface will increase, indicating that the energy localization effect is enhanced. However, it should be mentioned that as $k_t$ keeps increasing from $k_2$, it gradually approaches $k_1$, i.e., $|k_1 - k_t|$ becomes smaller. Consequently, the band-folding bandgap will become narrower, posing additional difficulties to obtain the topological interface mode for practical application. For the above reasons, $k_t$ is not recommended to be tuned too high as well. In summary, it can be concluded that the appropriate use of the stiffness tuning approach could enhance the wave localization effect, thus remarkably increase the output voltage of the topological meta-VEHs.

### B. Defect enhancement approach

Since both defect mode and topological interface mode have the capabilities to localize the elastic wave energy at the defect/interface, it is reasonable to integrate the defect mode with the topological interface mode to realize the megamerger. Thus, the second strategy proposed in this paper is to introduce a defect at the interface of a topological meta-VEH. In this way, the advantages of both the defect mode and the topological interface mode could be inherited in the topological metamaterial system for enhanced energy harvesting. Figure 10(a) illustrates the schematic of the defected topological meta-VEH. The defect is represented by a singular stiffness $k_d$ that varies from 1600 to 5200 N/m. Figure 10(b) depicts the effect of singular stiffness $k_d$ on the eigenfrequency and the output voltage of the

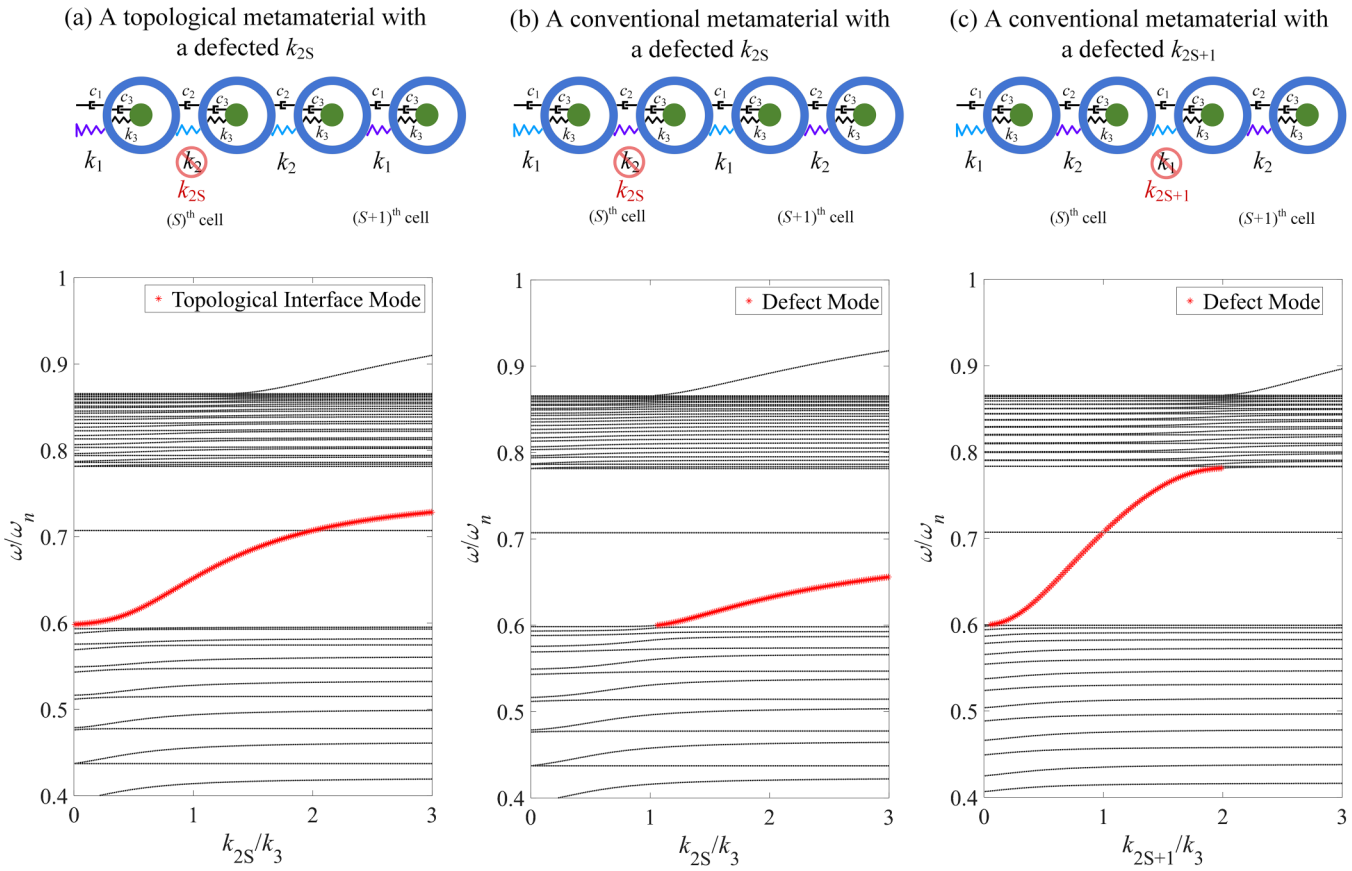


**FIG. 8.** Resonance peaks of defected metamaterials (30 cells, 60 modules): (a) a defected topological metamaterial (varying $k_{2S}$), (b) a defected conventional metamaterial (varying $k_{2S}$), and (c) a defected conventional metamaterial (varying $k_{2S+1}$).

topological meta-VEH. It is found in Fig. 10(b) that with the increase in $k_d$, the eigenfrequency increases, while the output voltage decreases. As reducing the singular stiffness $k_d$ at the interface can reduce the eigenfrequency and increase the output voltage simultaneously, it is obviously beneficial for low-frequency energy harvesting. By further plotting the displacement distributions for different singular stiffness $k_d$ in Fig. 10(c), it is found that a smaller $k_d$ helps enhance the energy localization effect, which explains why the output voltage is increased.

It should be mentioned that for the defect enhancement approach, the stiffness changes only at the interface while the other stiffnesses of the entire meta-VEH remain constant. However, in the stiffness tuning approach, the stiffnesses vary not only at the interface, but also in each unit cell of the entire system. The stiffness tuning approach is based on designing the band structure and topological interface mode of a purely topological meta-VEH. The decrease in stiffness $k_t$ can affect the topology property and the interface mode significantly. On the other hand, the defect enhancement approach is inspired by maximizing the wave localization effect through utilizing the defect mode and interface mode simultaneously. The change of stiffness $k_d$ may not change the topology property of the entire system. Thus, the reason that the decreasing stiffness may lead to different results for these two methods is due to the different underlying mechanisms. For a conventional defected meta-VEH, a decrease in stiffness at the interface can make the defect softer and concentrate more energy at the defect, leading to a larger output voltage. When the defect is introduced into the interface mode, this defect enhanced wave localization feature is inherited by the defected topological meta-VEH. Meanwhile, from Sec. IV B, it is found that the interface mode will always exist unless the stiffness at the interface becomes zero or infinity. In other words, integrating the defect mode with the topological interface mode at the interface edge is a feasible means to overcome the robustness problem of the defect mode itself. Thus, the defected topological meta-VEH attains a highly robust energy harvesting capability as compared to both the conventional defected meta-VEH and the purely topological meta-VEH. In general, a defected topological meta-VEH is promising to achieve robust and efficient vibration energy harvesting.

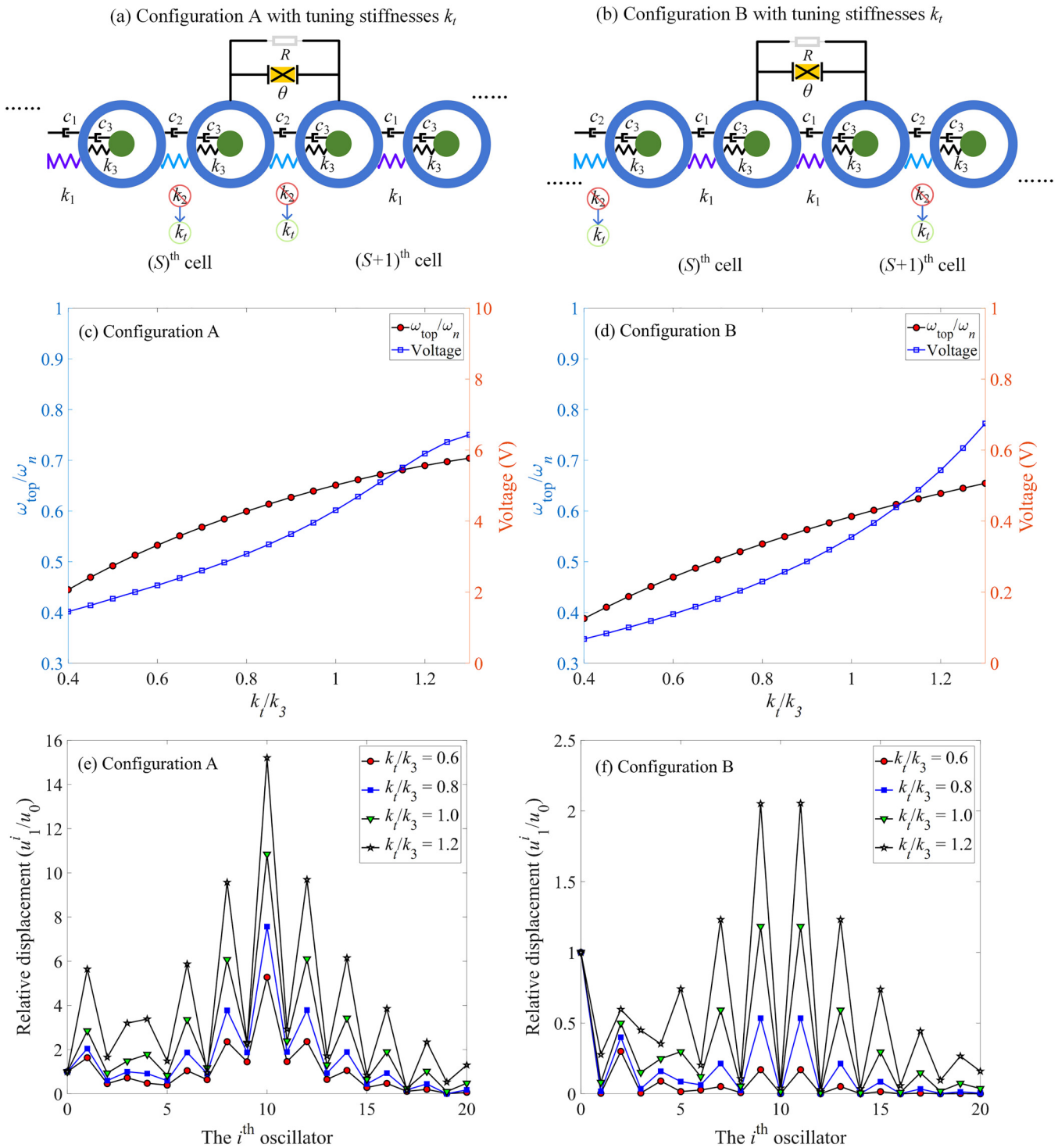


**FIG. 9.** Effect of stiffness $k_t$ on the topological interface mode and output voltage: (a) and (b) represent the models of configuration A and configuration B, respectively, (c) and (d) refer to the output voltage and eigenfrequency of topological interface mode for varying $k_t$, $\omega_{top}$ refers to the frequency of interface mode, (e) and (f) show the effect of stiffness $k_t$ on the displacement distribution of topological interface modes.

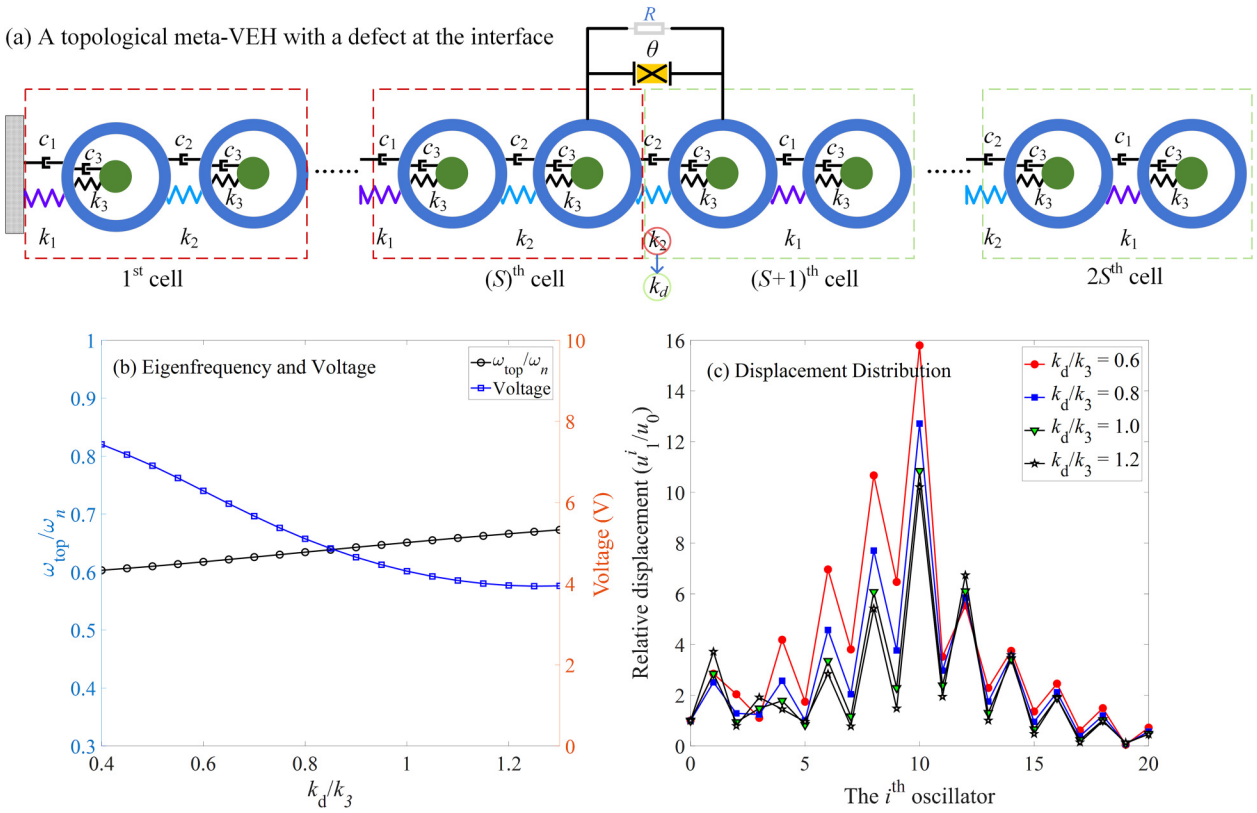


**FIG. 10.** A topological meta-VEH with a defected interface: (a) schematic, (b) effect of defected stiffness $k_d$ on the eigenfrequency of topological interface mode and the corresponding voltage output, and (c) displacement distributions for different $k_d$.

## VI. CONCLUSIONS

This paper has proposed a novel vibration energy harvester based on a locally resonant topological metamaterial. The governing equations and analytical solutions have been theoretically derived. The band structure and transmittance properties have been investigated. To ascertain the potential advantages of the topological meta-VEH, the wave localization and topological protection properties have been studied. Moreover, two different approaches to enhance the energy harvesting performance of the topological meta-VEH have been proposed. Through this analytical and numerical study, several useful findings have been obtained.

(1) The topological interface mode can be maintained at subwavelengths by the locally resonant topological metamaterial, which is favorable for low-frequency vibration energy harvesting.
(2) The wave localization property of the topological interface mode can concentrate the wave energy at the interface to help the energy harvester produce a large output voltage. Meanwhile, configuration A is more suitable for vibration energy harvesting, since it has a better wave localization capability.
(3) The topological protection makes the topological meta-VEH immune to the local defect, and the interface mode will always exist if the topology property keeps constant. Thus, as compared with the conventional defect meta-VEH, the topological meta-VEH exhibits a more robust energy harvesting performance.
(4) For the stiffness tuning approach, the energy localization property can be enhanced by optimizing the stiffness of the diatomic lattice, and, thus, the output voltage. For the defect enhancement method, it is revealed that integrating the defect mode and interface mode can significantly improve the energy localization function and the output voltage. Meanwhile, the defected topological meta-VEH still possesses the capability of topological protection, since the topology property is not changed by the defect. As a result, the defected topological meta-VEH is more suitable for a highly robust and efficient energy harvesting than the stiffness tuning approach.

## ACKNOWLEDGEMENTS

The author would like to acknowledge the financial support from the Natural Science Foundation of China (Grant No. 12002152), Natural Science Foundation of Jiangsu Province (Grant No. BK20190379), China Postdoctoral Science Foundation Funded Project (Grant No. 2020M681577), and a project funded by the Priority Academic Program Development of Jiangsu Higher Education Institutions.

## APPENDIX: BAND STRUCTURE AND TRANSMITTANCE ANALYSIS METHODS

### A. Method of calculating the band structure

The dashed box in Fig. 2 marks a unit cell of the metamaterial under investigation. $k_l$ and $k_r$ refer to the left and right spring constants, respectively, and $c_l$ and $c_r$ refer to the left and right damping terms in a unit cell, respectively. For the left metamaterial chain, $k_l = k_1$ and $k_r = k_2$. For the right metamaterial chain, $k_l = k_2$ and $k_r = k_1$. To theoretically derive the dispersion relation, the damping terms ($c_l$, $c_r$, and $c_3$), electromechanical coupling $\theta$, and the boundary conditions at the fixed end, free end, and conjunction are removed. Equation (1) is, thus, simplified as

$$\begin{cases} m_1\ddot{u}_1^{2i+1} + k_1(u_1^{2i+1} - u_1^{2i}) - k_2(u_1^{2i+2} - u_1^{2i+1}) + k_3(u_1^{2i+1} - u_2^{2i+1}) = 0, \\ m_2\ddot{u}_2^{2i+1} + k_3(u_2^{2i+1} - u_1^{2i+1}) = 0, \\ m_1\ddot{u}_1^{2i+2} + k_2(u_1^{2i+2} - u_1^{2i+1}) - k_1(u_1^{2i+3} - u_1^{2i+2}) + k_3(u_1^{2i+2} - u_2^{2i+2}) = 0, \\ m_2\ddot{u}_2^{2i+2} + k_3(u_2^{2i+2} - u_1^{2i+2}) = 0. \end{cases} \tag{A1}$$

Similarly, Eq. (4) is also simplified as

$$\begin{cases} m_1\ddot{u}_1^{2i+1} + k_2(u_1^{2i+1} - u_1^{2i}) - k_1(u_1^{2i+2} - u_1^{2i+1}) + k_3(u_1^{2i+1} - u_2^{2i+1}) = 0, \\ m_2\ddot{u}_2^{2i+1} + k_3(u_2^{2i+1} - u_1^{2i+1}) = 0, \\ m_1\ddot{u}_1^{2i+2} + k_1(u_1^{2i+2} - u_1^{2i+1}) - k_2(u_1^{2i+3} - u_1^{2i+2}) + k_3(u_1^{2i+2} - u_2^{2i+2}) = 0, \\ m_2\ddot{u}_2^{2i+2} + k_3(u_2^{2i+2} - u_1^{2i+2}) = 0. \end{cases} \tag{A2}$$

Based on Bloch's theorem, the displacements of masses in the $(2i+1)$th and $(2i+2)$th unit cells are assumed in the harmonic wave forms as

$$\begin{cases} u_1^{2i+1} = Ae^{j(qx-\omega t)}, \\ u_1^{2i+2} = Be^{j(qx+qL-\omega t)}, \\ u_2^{2i+1} = Ce^{j(qx-\omega t)}, \\ u_2^{2i+2} = De^{j(qx+qL-\omega t)}, \end{cases} \tag{A3}$$

where $A$, $B$, $C$, and $D$ are complex wave amplitudes, $q$ is the wave number, $\omega$ is the angular frequency, $j$ is the imaginary number, and $L$ is the lattice constant. Substituting Eq. (A3) into Eqs. (A1) and (A2) yields

$$\begin{cases} -m_1\omega^2 A + k_l(A - Be^{-jqL}) - k_r(Be^{jqL} - A) + k_3(A - C) = 0, \\ -m_2\omega^2 C + k_3(C - A) = 0, \\ -m_1\omega^2 B + k_r(B - Ae^{-jqL}) - k_l(Ae^{jqL} - B) + k_3(B - D) = 0, \\ -m_2\omega^2 D + k_3(D - B) = 0. \end{cases} \tag{A4}$$

Arranging Eq. (A4) in the matrix form yields

$$\mathbf{Tp} = \mathbf{0}, \tag{A5}$$

where

$$\mathbf{T} = \begin{bmatrix} -m_1\omega^2 + k_l + k_r + k_3 & -k_le^{-jqL} - k_re^{jqL} & -k_3 & 0 \\ -k_3 & 0 & -m_2\omega^2 + k_3 & 0 \\ -k_re^{-jqL} - k_le^{jqL} & -m_1\omega^2 + k_l + k_r + k_3 & 0 & -k_3 \\ 0 & -k_3 & 0 & k_3 - m_2\omega^2 \end{bmatrix}, \quad \mathbf{p} = [A \quad B \quad C \quad D]^T. \tag{A6}$$

Letting the determinant of the coefficient matrix of Eq. (A6) equal to zero, i.e., $\det(\mathbf{T}) = 0$, gives the dispersion relation of the metamaterial.

### B. Method of calculating the transmittance

To calculate the transmittance of the proposed topological meta-VEH, the governing equations [from Eqs. (1)–(7)] should be solved simultaneously. Assuming that the system is excited by a harmonic excitation at the fixed end $[u_0(t) = u_0 \times \sin(\omega t)]$, the Laplace transformation method is employed to transform the governing equations into the frequency domain. First, the relation between the displacement amplitudes of the outer and inner masses is obtained as

$$u_2^{i+1} = \frac{j\omega c_3 + k_3}{-\omega^2 m_2 + j\omega c_3 + k_3} u_1^{i+1} \qquad (i = 0 \sim 2S - 1). \tag{B1}$$

Substituting Eq. (B1) back into Eqs. (1)–(6), we have

$$\begin{cases} \begin{bmatrix} a_2 u_1^{2i+1} + a_3 u_1^{2i+2} = k_1 u_1^0 \\ a_3 u_1^{2i+1} + a_2 u_1^{2i+2} + a_1 u_1^{2i+3} = 0 \end{bmatrix} & (i = 0), \\ \begin{bmatrix} a_1 u_1^{2i} + a_2 u_1^{2i+1} + a_3 u_1^{2i+2} = 0 \\ a_3 u_1^{2i+1} + a_2 u_1^{2i+2} + a_1 u_1^{2i+3} = 0 \end{bmatrix} & (i = 1 \sim S - 2), \\ \begin{bmatrix} a_1 u_1^{2i} + a_2 u_1^{2i+1} + a_3 u_1^{2i+2} = 0 \\ a_3 u_1^{2i+1} + (a_2 - k_1 - j\omega c_1 + k_2 + j\omega c_2 + a_5) u_1^{2i+2} + (a_3 - a_5) u_1^{2i+3} = 0 \end{bmatrix} & (i = S - 1), \\ \begin{bmatrix} (a_3 - a_5) u_1^{2i} + (a_2 + a_5) u_1^{2i+1} + a_1 u_1^{2i+2} = 0 \\ a_1 u_1^{2i+1} + a_2 u_1^{2i+2} + a_3 u_1^{2i+3} = 0 \end{bmatrix} & (i = S), \\ \begin{bmatrix} a_3 u_1^{2i} + a_2 u_1^{2i+1} + a_1 u_1^{2i+2} = 0 \\ a_1 u_1^{2i+1} + a_2 u_1^{2i+2} + a_3 u_1^{2i+3} = 0 \end{bmatrix} & (i = S + 1 \sim 2S - 2), \\ \begin{bmatrix} a_3 u_1^{2i} + a_2 u_1^{2i+1} + a_1 u_1^{2i+2} = 0 \\ a_1 u_1^{2i+1} + a_2 u_1^{2i+2} = 0 \end{bmatrix} & (i = 2S - 1), \end{cases} \tag{B2}$$

where

$$a_1 = -(j\omega c_1 + k_1),\ a_2 = (-\omega^2 m_1 + j\omega c_1 + j\omega c_2 + j\omega c_3 + k_1 + k_2 + k_3 + a_4),\ \text{and}\ a_3 = -(j\omega c_2 + k_2),$$
$$a_4 = -\frac{(j\omega c_3 + k_3)^2}{-\omega^2 m_2 + j\omega c_3 + k_3},\ a_5 = \frac{j\omega R\theta^2}{1 + j\omega R C_p}. \tag{B3}$$

From Eq. (7), the output voltage and power can be obtained as

$$\begin{cases} v = -\dfrac{j\omega R\theta}{1 + j\omega R C_p} u_S, \\ P = \dfrac{v^2}{R} = \left( -\dfrac{j\omega R\theta}{1 + j\omega R C_p} \right)^2 \dfrac{u_S^2}{R}, \end{cases} \tag{B4}$$

where $u_S = u_1^{2S+1} - u_1^{2S}$.

By solving Eq. (B2), the displacement amplitude of the system can be obtained. The transmittance of this system can be defined and calculated as

$$\tau = \frac{|u_1^{4S} + u_1^0|}{|u_1^0|}. \tag{B5}$$

## DATA AVAILABILITY

The data that support the findings of this study are available within the article.

## REFERENCES


[1] S. Priya and D. J. Inman, *Energy Harvesting Technologies* (Springer, 2009).
[2] H. Liu, J. Zhong, C. Lee, S. W. Lee, and L. Lin, "A comprehensive review on piezoelectric energy harvesting technology: Materials, mechanisms, and applications," Appl. Phys. Rev. **5**(4), 041306 (2018).
[3] H. Zhou, Y. Zhang, Y. Qiu, H. Wu, W. Qin, Y. Liao, and H. Cheng, "Stretchable piezoelectric energy harvesters and self-powered sensors for wearable and implantable devices," Biosens. Bioelectron. **168**, 112569 (2020).
[4] A. Erturk and D. J. Inman, *Piezoelectric Energy Harvesting* (John Wiley & Sons, 2011).
[5] S. C. Stanton, C. C. McGehee, and B. P. Mann, "Reversible hysteresis for broadband magnetopiezoelastic energy harvesting," Appl. Phys. Lett. **95**(17), 174103 (2009).
[6] A. Erturk, J. Hoffmann, and D. J. Inman, "A piezomagnetoelastic structure for broadband vibration energy harvesting," Appl. Phys. Lett. **94**(25), 254102 (2009).
[7] S. Zhou and L. Zuo, "Nonlinear dynamic analysis of asymmetric tristable energy harvesters for enhanced energy harvesting," Commun. Nonlinear Sci. Numer. Simulat. **61**, 271–284 (2018).
[8] G. Hu, L. Tang, R. Das, and P. Marzocca, "A two-degree-of-freedom piezoelectric energy harvester with stoppers for achieving enhanced performance," Int. J. Mech. Sci. **149**, 500–507 (2018).
[9] L. Q. Chen and W. A. Jiang, "Internal resonance energy harvesting," J. Appl. Mech. **82**(3), 031004 (2015).

[10]C. Lan, L. Tang, W. Qin, and L. Xiong, "Magnetically coupled dual-beam energy harvester: Benefit and trade-off," J. Intell. Mater. Syst. Struct. **29**(6), 1216–1235 (2018).
[11]H. Wu, L. Tang, Y. Yang, and C. K. Soh, "Development of a broadband nonlinear two-degree-of-freedom piezoelectric energy harvester," J. Intell. Mater. Syst. Struct. **25**(14), 1875–1889 (2014).
[12]M. F. Daqaq, R. Masana, A. Erturk, and D. Dane Quinn, "On the role of nonlinearities in vibratory energy harvesting: A critical review and discussion," Appl. Mech. Rev. **66**(4), 040801 (2014).
[13]J. Wang and W. H. Liao, "Attaining the high-energy orbit of nonlinear energy harvesters by load perturbation," Energy Convers. Manage. **192**, 30–36 (2019).
[14]C. Lan, Z. Chem, G. Hu, Y. Liao, and W. Qin, "Achieve frequency-self-tracking energy harvesting using a passively adaptive cantilever beam," Mech. Syst. Signal Process. **156**, 107672 (2021).
[15]S. Gonella, A. C. To, and W. K. Liu, "Interplay between phononic bandgaps and piezoelectric microstructures for energy harvesting," J. Mech. Phys. Solids **57**(3), 621–633 (2009).
[16]K. Mikoshiba, J. M. Manimala, and C. Sun, "Energy harvesting using an array of multifunctional resonators," J. Intell. Mater. Syst. Struct. **24**(2), 168–179 (2013).
[17]L. Shen, J. Wu, S. Zhang, Z. Liu, and J. Li, "Low-frequency vibration energy harvesting using a locally resonant phononic crystal plate with spiral beams," Mod. Phys. Lett. B **29**(1), 1450259 (2015).
[18]G. Hu, L. Tang, and R. Das, "Internally coupled metamaterial beam for simultaneous vibration suppression and low frequency energy harvesting," J. Appl. Phys. **123**(5), 055107 (2018).
[19]L. Y. Wu, L. W. Chen, and C. M. Liu, "Acoustic energy harvesting using resonant cavity of a sonic crystal," Appl. Phys. Lett. **95**(1), 013506 (2009).
[20]M. Carrara, M. Cacan, J. Toussaint, M. Leamy, M. Ruzzene, and A. Erturk, "Metamaterial-inspired structures and concepts for elastoacoustic wave energy harvesting," Smart Mater. Struct. **22**(6), 065004 (2013).
[21]M. Carrara, M. Cacan, M. Leamy, M. Ruzzene, and A. Erturk, "Dramatic enhancement of structure-borne wave energy harvesting using an elliptical acoustic mirror," Appl. Phys. Lett. **100**(20), 204105 (2012).
[22]S. Tol, F. L. Degertekin, and A. Erturk, "Gradient-index phononic crystal lens-based enhancement of elastic wave energy harvesting," Appl. Phys. Lett. **109**(6), 063902 (2016).
[23]G. Ma, M. Xiao, and C. T. Chan, "Topological phases in acoustic and mechanical systems," Nat. Rev. Phys. **1**, 281 (2019).
[24]C. He, X. Ni, H. Ge, X. C. Sun, Y. B. Chen, M. H. Lu, and Y. F. Chen, "Acoustic topological insulator and robust one-way sound transport," Nat. Phys. **12**(12), 1124–1129 (2016).
[25]P. Wang, L. Lu, and K. Bertoldi, "Topological phononic crystals with one-way elastic edge waves," Phys. Rev. Lett. **115**(10), 104302 (2015).
[26]R. Chaunsali, E. Kim, A. Thakkar, P. G. Kevrekidis, and J. Yang, "Demonstrating an in situ topological band transition in cylindrical granular chains," Phys. Rev. Lett. **119**(2), 024301 (2017).
[27]L. Fan, Y. He, X. A. Chen, and X. Zhao, "Acoustic energy harvesting based on the topological interface mode of 1D phononic crystal tube," Appl. Phys. Express **13**(1), 017004 (2019).
[28]W. Su, J. R. Schrieffer, and A. J. Heeger, "Solitons in polyacetylene," Phys. Rev. Lett. **42**(25), 1698 (1979).
[29]J. Yin, M. Ruzzene, J. Wen, D. Yu, L. Cai, and L. Yue, "Band transition and topological interface modes in 1D elastic phononic crystals," Sci. Rep. **8**(1), 6806 (2018).
[30]Z. Muhammad, W. & Lim, and C. W, "Topological edge modeling and localization of protected interface modes in 1D phononic crystals for longitudinal and bending elastic waves," Int. J. Mech. Sci. **159**, 359–372 (2019).
[31]D. Zhao, M. Xiao, C. W. Ling, C. T. Chan, and K. H. Fung, "Topological interface modes in local resonant acoustic systems," Phys. Rev. B **98**(1), 014110 (2018).
[32]M. Xiao, G. Ma, Z. Yang, P. Sheng, Z. Q. Zhang, and C. T. Chan, "Geometric phase and band inversion in periodic acoustic systems," Nat. Phys. **11**(3), 240–244 (2015).
[33]L. Fan, Y. He, X. Zhao, and X. A. Chen, "Subwavelength and broadband tunable topological interface state for flexural wave in one-dimensional locally resonant phononic crystal," J. Appl. Phys. **127**(23), 235106 (2020).